SUPPLEMENTARY MATERIALS

Structural and Mechanistic Studies of the Rare Myristoylation Signal of the Feline Immunodeficiency Virus

Janae B. Brown[1], Holly R. Summers[1], Lola A. Brown[1], Jan Marchant[1], Paige N. Canova[1], Colin T. O'Hern[1], Sophia T. Abbott[1], Constance Nyaunu[1], Simon Maxwell[1], Talayah Johnson[1], Morgan B. Moser[1], Sherimay D. Ablan[2], Hannah Carter[2], Eric O. Freed[2,*], Michael F. Summers[1]

[1]*Howard Hughes Medical Institute and Department of Chemistry and Biochemistry, University of Maryland Baltimore County, Baltimore, MD 21250, USA*

[2]*Virus–Cell Interaction Section, HIV Dynamics and Replication Program, National Cancer Institute at Fredrick, Fredrick, MD 21702-1201, USA*

Supplementary Figure Captions

Figure S1. Truncation does not influence the structure of FIV MA. HSQC spectra of full-length FIV MA (black) and truncated FIV MA (red) are in good agreement, suggestive of the retained structure upon truncation. Similarly, the spectrum of truncated FIV myr(-)MA (blue) is very similar to that of the full-length (orange). Signals absent in the truncated spectra correspond to amino acid residues removed from the carboxy-terminal tail. Small chemical shift differences are observed in residues near the site of C-terminal truncation and within the C-terminal 6X His tag used for affinity chromatography purification.

Figure S2. The X-ray crystallography-derived structure of human NMT (PDB ID: 5O9V) features a substrate sequence to be myristoylated (orange) and myristoyl CoA (cyan). Mutations in the feline NMT sequence are highlighted in red. These mutations are on the surface of the protein and are removed from the sites for NMT substrate binding (blue), myristoyl CoA binding site (lime), and the catalytic region (magenta).

Figure S3. MA chemical shifts are insensitive to varied protein concentration and pH. (a) Superposed ^{1}H-^{15}N HSQC of MA at pH 8.0 (red), pH 7.0 (grey), and pH 6.0 (blue) demonstrate that the signals are not pH sensitive. Residue His 122 belongs to the metal affinity chromatography tag. (b) Concentration does not impact MA chemical shifts, as illustrated in the overlaid HSQC spectra of MA at pH 6.0 and 50 μM (red), 100 μM (green), 150 μM (purple), 225 μM (blue), and 920 μM (lime). (c) myr(-)MA signals at pH 8.0 (cyan), pH 7.0 (purple), pH 6.0 (green), and pH 5.0 (red) are not perturbed by pH but amide signals are recovered at low pH.

Figure S4. FIV myr(-)MA is spontaneously deamidated. (a) A schematic of the sign inversion of N3-Cα (positive, black) and -Cβ (negative, red) before deamidation to the deamidation product iso-

aspartate 3 (iD3) (negative/red Cα, positive/black Cβ) relative to the amide of G4 (grey) observed in the HNCACB. (b) HNCACB strips with dashed lines illustrating the correlations between iD3 and G4 in the deamidated myr(-)MA. Specifically, G4 shows the intensity inversion to the iD3-Cα and -Cβ chemical shifts.

Figure S5. Overlaid ^{1}H-^{13}C HMQC spectra of [U-^{13}C] MA (black) and [^{12}C-myr, ^{13}C-MA] MA (red) show signals that belong to the myristoyl moiety. Lower levels reveal well-resolved myristoyl moiety signals (top and middle) which are very similar to those observed in the HMQC of FIV (^{13}C-myr)MA Q5A/G6S ^{12}C (bottom).

Figure S6. A representative region of the overlaid [^{1}H-^{15}N] HSQC spectra of myr(-)MA (cyan) and myr(-)MA^{NOS} (brown) collected at pH 5.0. Differences are localized to the N-termini (residues Asn 3 – Met 11).

Figure S7. XNOE data for myr(-)MA (cyan) and myr(-)MA^{NOS} (brown) indicate that XNOE values for most residues of these constructs were similar with the exception of the N-terminus. Helices are indicated by grey backgrounds. The brown asterisk represents Ser 6 in myr(-)MA^{NOS} that leads helix-I but does not include the grey shade because helix-I is initiated with Arg 7 in myr(-)MA.

Figure S8. Results of virus release assays performed by transfection of 293T cells with plasmids containing WT, G2A (negative control), and NOS mutations. Levels of p24 in virions were quantified relative to cellular levels of p24 and p50 (full-length Gag). The efficiency of NOS virus release from human 293T cells is consistent with that observed for feline kidney (CrFK) cells.

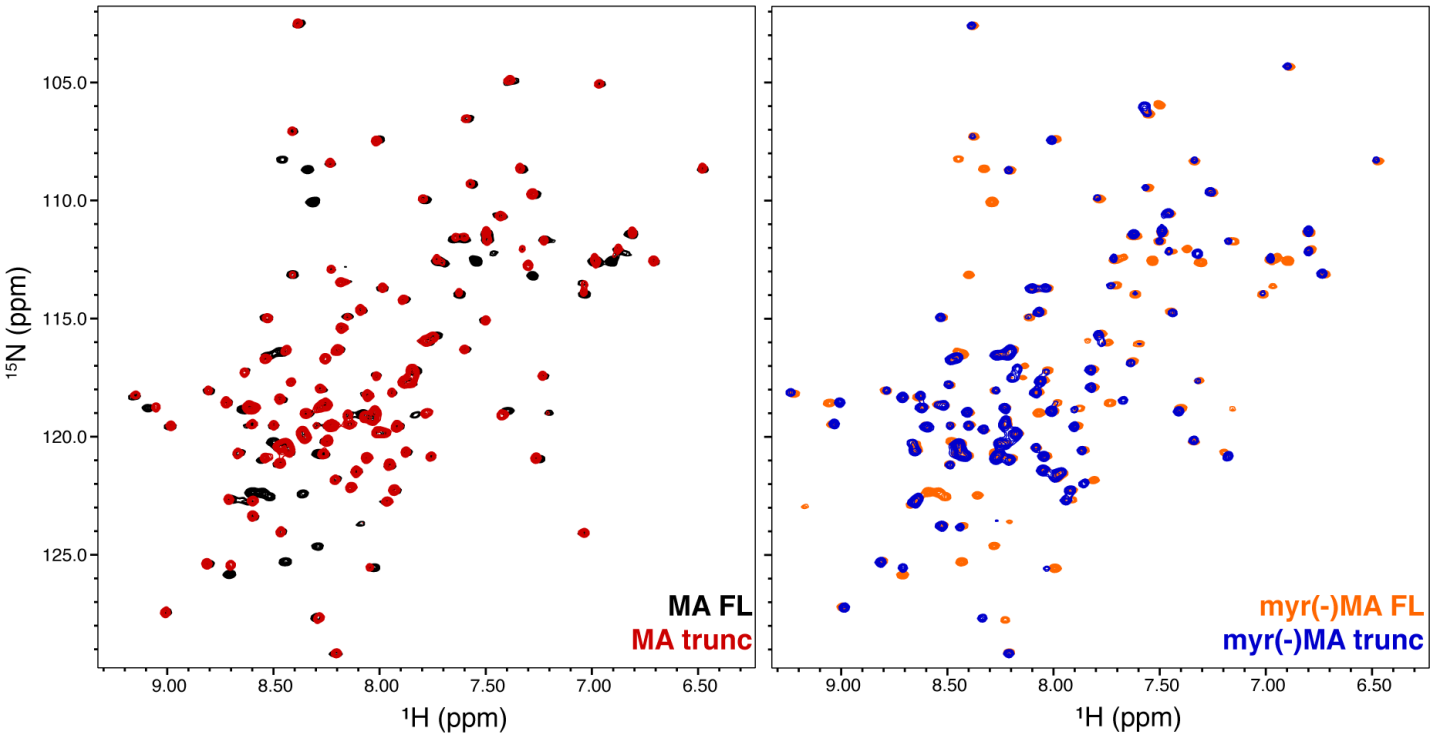
105.0
110.0
115.0
120.0
125.0
^{15}N (ppm)
9.00
8.50
8.00
7.50
7.00
6.50
^{1}H (ppm)
MA FL
MA trunc
myr(-)MA FL
myr(-)MA trunc

Figure S1.

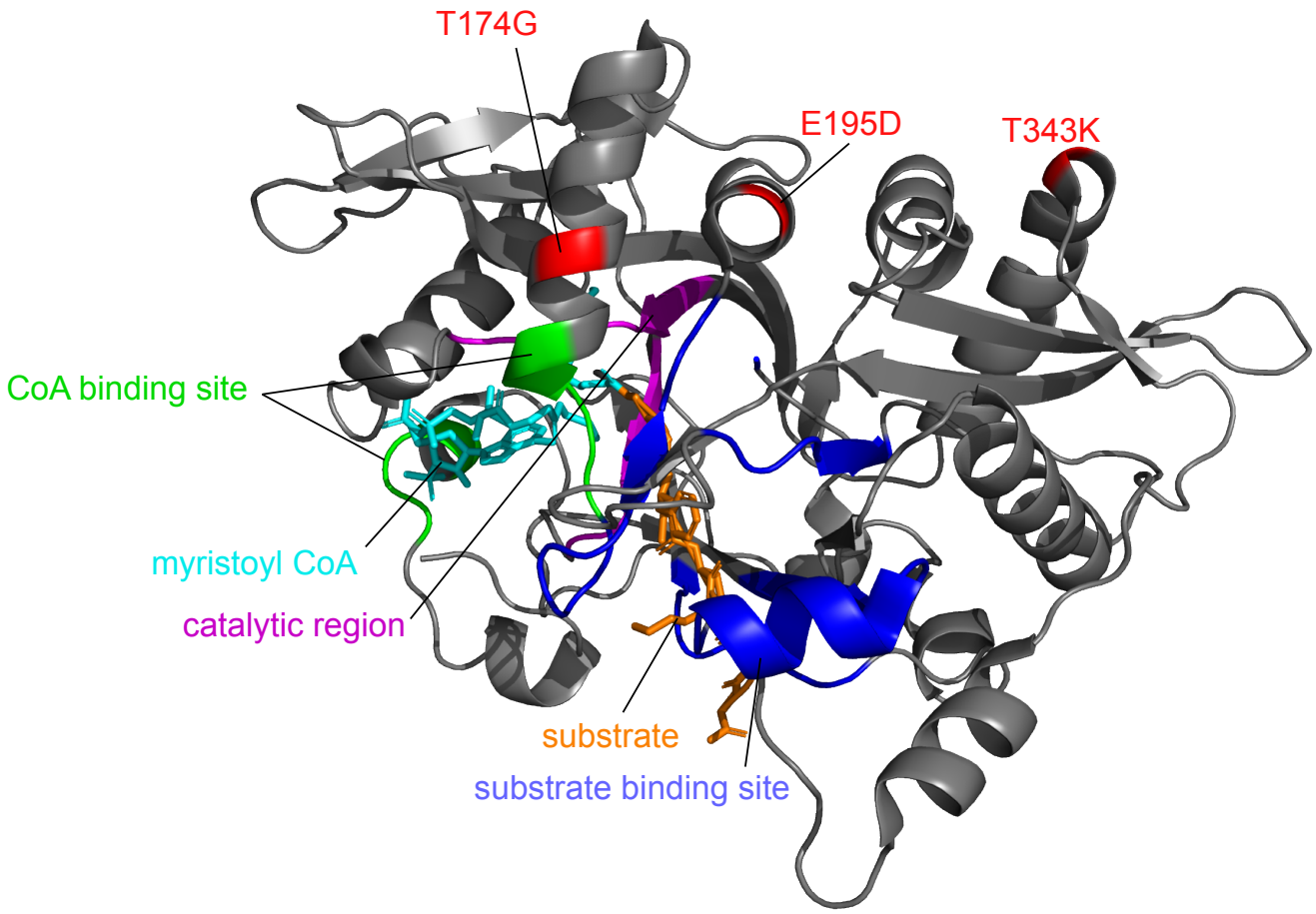
T174G
E195D
T343K
CoA binding site
myristoyl CoA
catalytic region
substrate
substrate binding site

Figure S2.

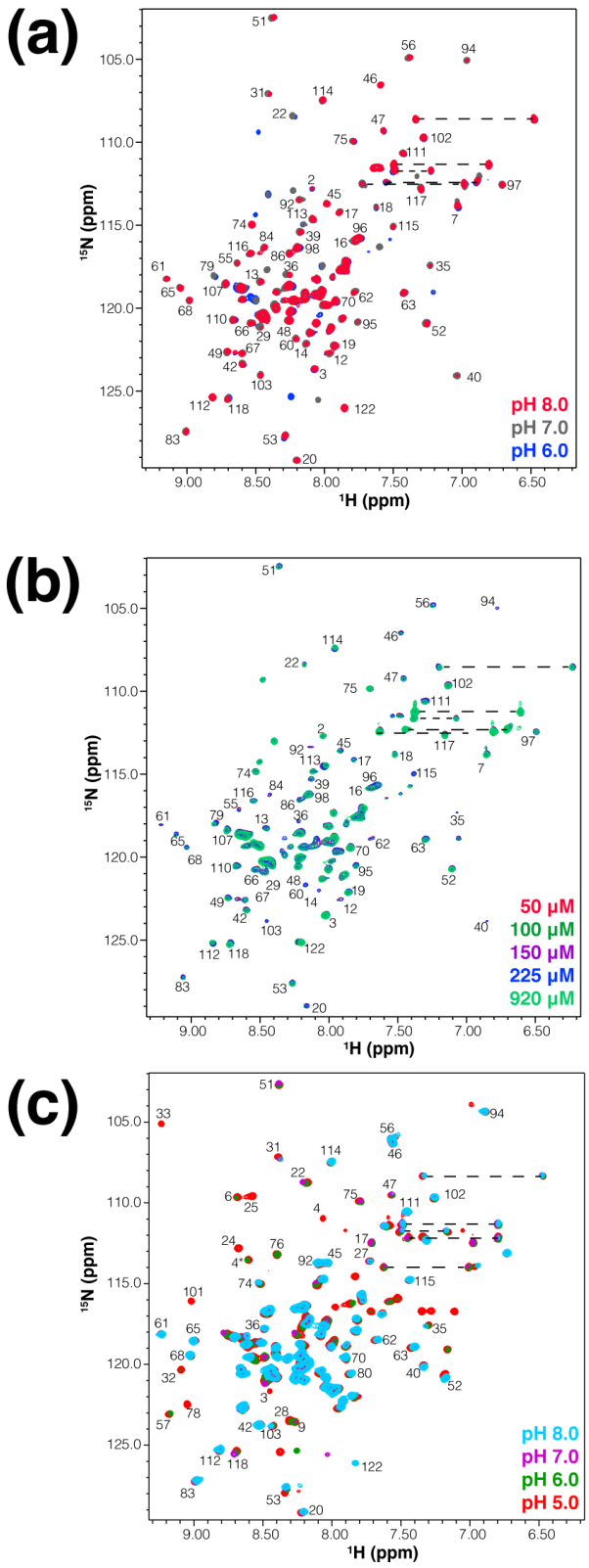
(a)
pH 8.0
pH 7.0
pH 6.0
(b)
50 µM
100 µM
150 µM
225 µM
920 µM
(c)
pH 8.0
pH 7.0
pH 6.0
pH 5.0
¹⁵N (ppm)
¹H (ppm)

Figure S3.

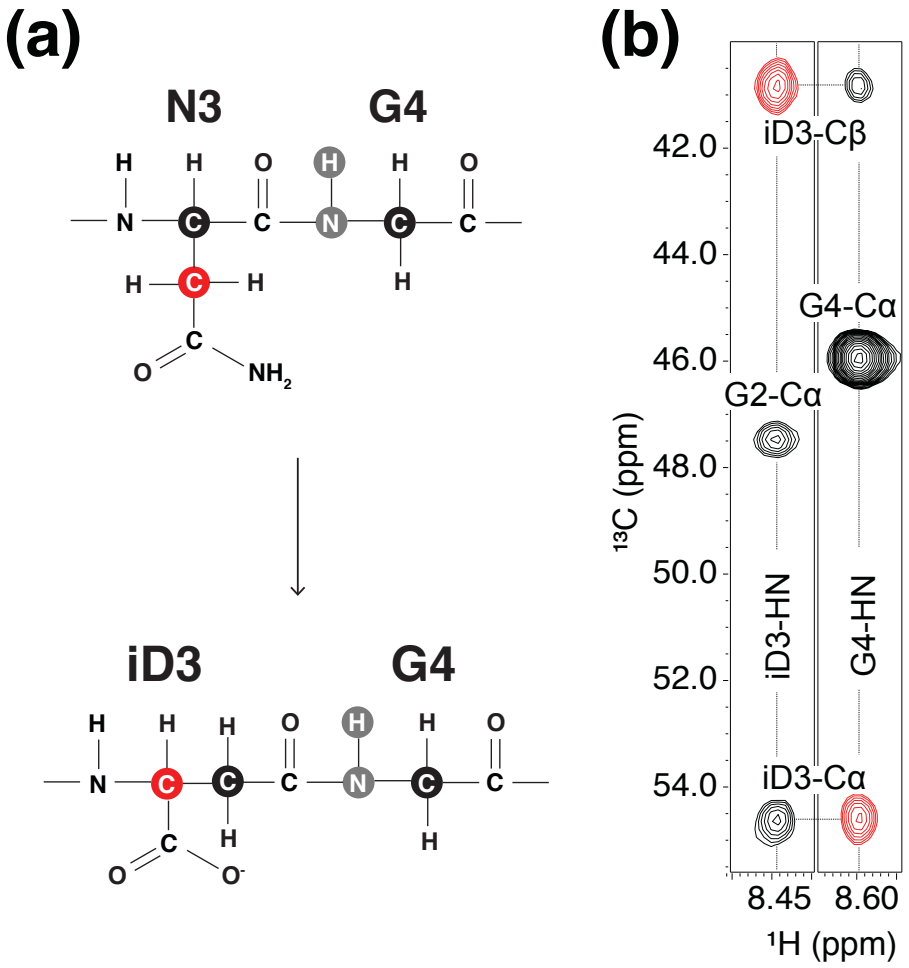
(a)
N3
G4
iD3
G4
(b)
iD3-Cβ
G4-Cα
G2-Cα
iD3-HN
G4-HN
iD3-Cα
42.0
44.0
46.0
48.0
50.0
52.0
54.0
13C (ppm)
8.45
8.60
1H (ppm)

Figure S4.

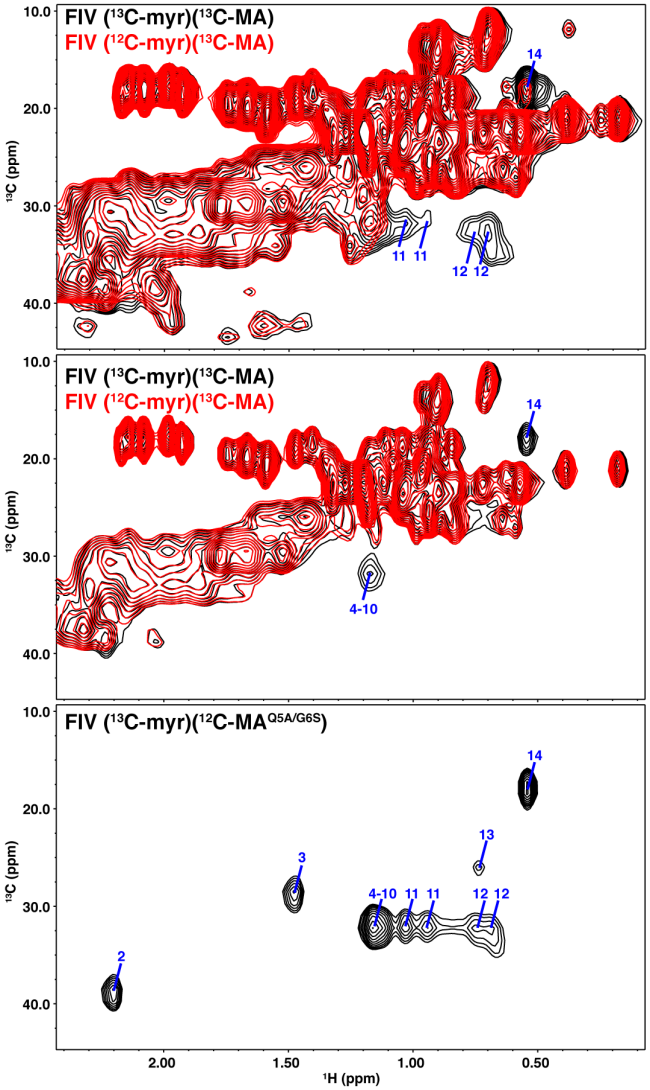
FIV (^{13}C-myr)(^{13}C-MA)
FIV (^{12}C-myr)(^{13}C-MA)
14
11 11
12 12
FIV (^{13}C-myr)(^{13}C-MA)
FIV (^{12}C-myr)(^{13}C-MA)
14
4-10
FIV (^{13}C-myr)(^{12}C-MA$^{Q5A/G6S}$)
14
13
3
4-10 11 11
12 12
2
^{13}C (ppm)
^{1}H (ppm)
10.0
20.0
30.0
40.0
2.00
1.50
1.00
0.50

Figure S5.

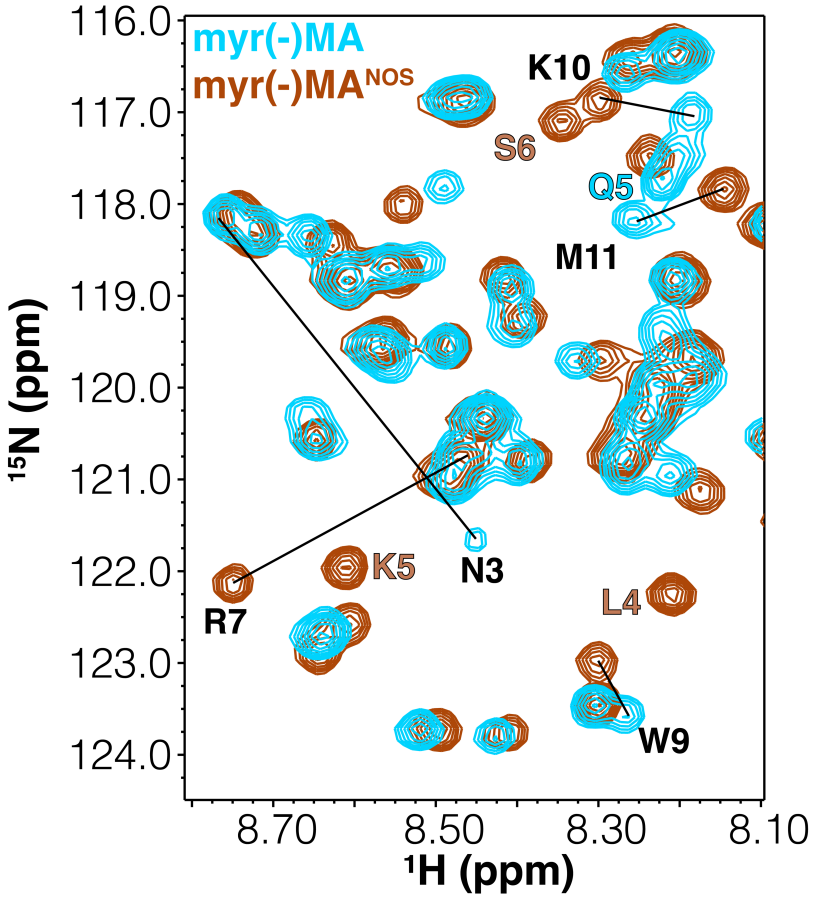
myr(-)MA
myr(-)MA^NOS
K10
S6
Q5
M11
N3
K5
R7
L4
W9
116.0
117.0
118.0
119.0
120.0
121.0
122.0
123.0
124.0
15N (ppm)
8.70
8.50
8.30
8.10
1H (ppm)

Figure S6.

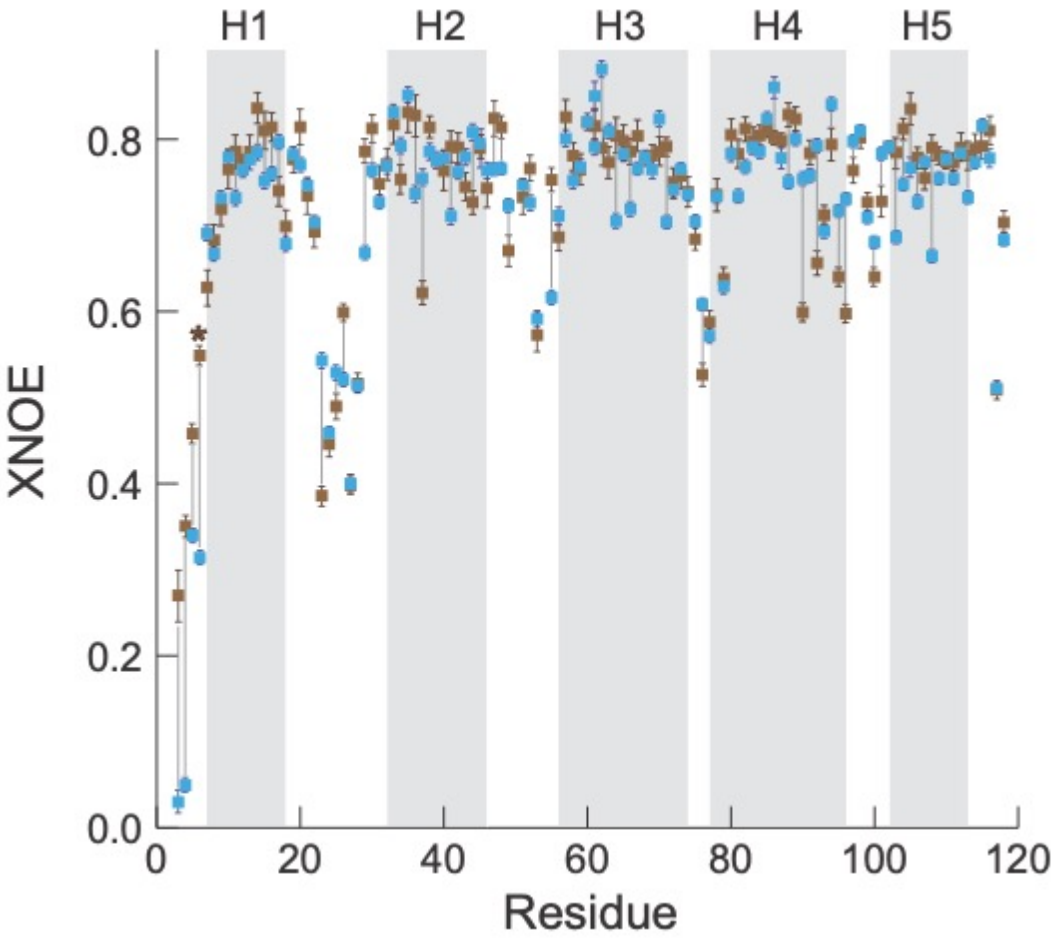

Figure S7.

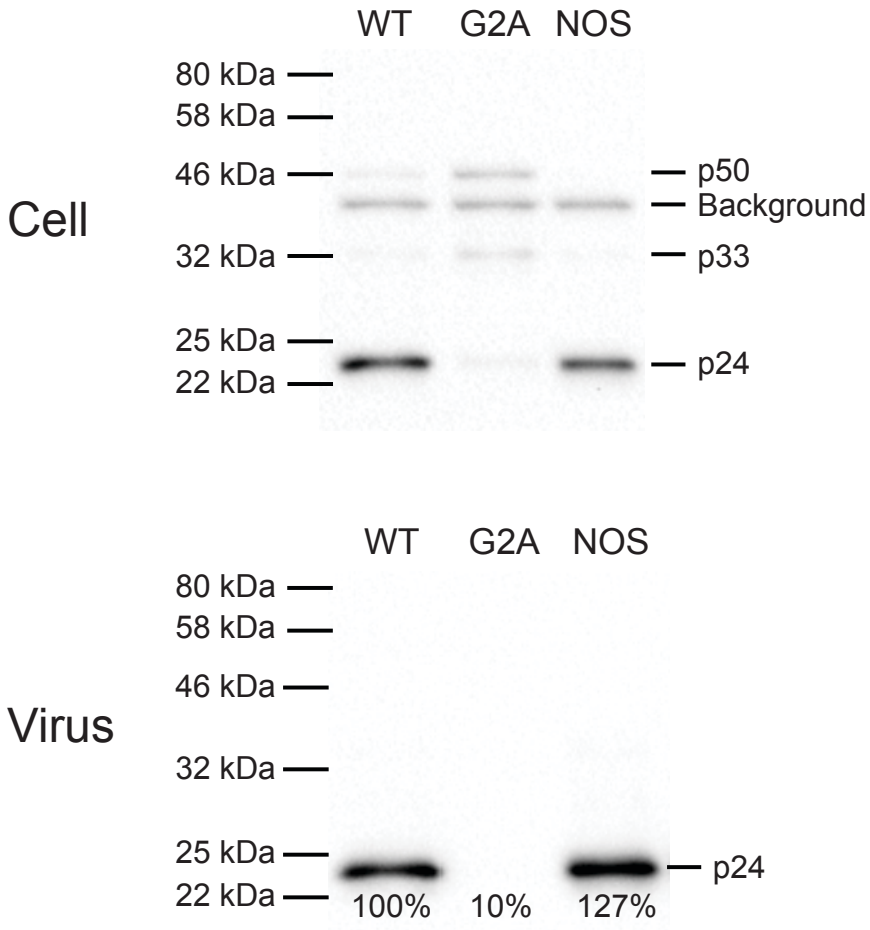
WT
G2A
NOS
Cell
80 kDa
58 kDa
46 kDa
32 kDa
25 kDa
22 kDa
p50
Background
p33
p24
WT
G2A
NOS
Virus
80 kDa
58 kDa
46 kDa
32 kDa
25 kDa
22 kDa
p24
100%
10%
127%

Figure S8.